JOURNAL OF CATALYSIS 128, 13–22 (1991)

The Effect of Ca^{2+} and Mg^{2+} Ions on the Formation of Electron-Deficient Palladium–Proton Adducts in Zeolite Y

ZONGCHAO ZHANG, TIM T. WONG, AND WOLFGANG M. H. SACHTLER

V. N. Ipatieff Laboratory, Center for Catalysis and Surface Science, Northwestern University, Evanston, Illinois 60208

Received May 10, 1990; revised October 1, 1990

FTIR spectra of adsorbed CO on Pd particles in supercages of zeolite Y show that positively charged Pd_n clusters are formed when the concentration of protons in the supercages is high and thereby confirm our hypothesis that $[Pd_nH]^+$ adducts are the "electron-deficient" palladium clusters that are responsible for catalytic superactivity. The formation of such adducts is favored by a high concentration of divalent charge-compensating ions, for example, Mg^{2+} or Ca^{2+}. Carbon monoxide displaces the protons from the $[Pd_nH]^+$ adducts; this leads to an increase of the IR band due to supercage O_Z–H groups. Simultaneously the $Pd_n(CO)_x$ entities migrate through the supercage channels and coalesce with each other. Temperature-programmed reduction (TPR) shows that substituting Na^+ by Mg^{2+} ions results in a downward shift by 70°C of the TPR peak for Pd^{2+} reduction. This suggests that the divalent ions preferentially populate sodalite cages and hexagonal prisms, thus preventing the migration of Pd^{2+} ions into these positions. During reduction, both Pd_n clusters and protons are formed in supercages, setting the stage for the formation of the $[Pd_nH]^+$ adducts.

I. INTRODUCTION

Zeolite-supported metals display high catalytic activity for the isomerization of alkanes, for example, *n*-pentane and *n*-hexane (*1, 2*). Numerous studies document a strong promoting effect of multivalent cations, such as Mg^{2+} and Ca^{2+}, or rare earth cations on the isomerization and hydrogenolysis activity (*3–8*). The nature of this promoting effect is the main subject of the present paper. As such catalysts are conventionally prepared by a sequence of three steps, viz., ion exchange, calcination, and reduction with hydrogen, they generally exhibit *bifunctionality* toward reacting gases; i.e., two types of active sites are exposed:

(1) *metal* sites, e.g., reduced Pt or Pd particles; and

(2) *acid* sites. These include protons of high Brønsted acidity, which are formed in the reduction step. In addition, Lewis acid sites are usually generated by dehydroxylation at high temperature. Furthermore, Brønsted acidity can be introduced by hydrolysis of multivalent cations such as La^{3+} ions (*9–11*).

Promoting effects of nonreducible multivalent charge-compensating ions in zeolites can thus be attributed to the metal function or the acid function or both. Most authors assume that the nonreducible multivalent ions alter the acidity of the zeolite supports in the bifunctional scheme (*12–15*). However, Figueras *et al.* reported that for a purely metal catalyzed reaction, such as benzene hydrogenation, the activities of PdCaY and PdMgY exceed that of PdNaY by factors of 2 and 3, respectively (*16*). Likewise, Mays *et al.* showed that multivalent ions increase the activity and stability of zeolite-supported Pd for the hydrogenation of diethylbenzene, which is also a metal-catalyzed reaction (*17*).

Recent results of this laboratory suggest, however, that the sharp distinction between metal function and Brønsted acid function in zeolite-supported metals may be a mis-

0021-9517/91 $3.00

leading simplification (*18*). Protons which are formed during the reduction of Pd, for example, with hydrogen

$$Pd^{2+} + H_2 \rightarrow Pd^0 + 2\,H^+,$$

can be attached to oxygen ions of the zeolite matrix, O_Z, and display strong Brønsted acidity. The same protons can, however, also interact with metal particles, forming positively charged adducts:

$$Pd_n + H^+ + O_Z \rightarrow Pd_n\text{--}H^+\text{--}O_Z \rightarrow [Pd_nH]^+\,O_Z.$$

In these $[Pd_nH]^+$ adducts the positive charge is distributed between metal and hydrogen atoms; using a definition by Boudart, the metal thus becomes "electron-deficient" (*19*). For the conversion of neopentane, it has been shown that electron-deficient Pt and Pd particles in zeolites display a much higher catalytic activity per exposed metal site than neutral Pt or Pd particles (*18, 19*).

In recent work, it was further shown that neutralization of the acid sites drastically reduces the activity of the metal sites (*18*). This neutralization can be achieved by exchanging the protons with alkali cations after reduction or by retaining part of the ammine ligands of the original Pt or Pd tetraammine complexes. Other recent results showed that introduction of CO_2 in MgY and CaY increases the acidity and, as a result, enhances the activity for isooctane hydrogenolysis (*12, 20, 21*).

Highly electron-deficient Pd particles (with Pd^+ as the limiting case) have been detected previously by ESR in zeolite NaY and CaY after reduction with H_2 (*20–24*). Using CO as a probing molecule, our recent studies demonstrated the potential of FTIR for monitoring the change of chemical interaction and physical morphology of metal particles such as Pd and Rh in NaY zeolite support (*22, 25–27*). In the present study, FTIR spectroscopy is used to determine the chemical nature of highly electron-difficient Pd particles in MgY and CaY zeolites and to study the neutralization effect of ammine ligands retained during controlled calcination.

II. EXPERIMENTAL

A. Sample Preparation

$M^{2+}Y$ (M^{2+} = Mg^{2+} or Ca^{2+}) zeolite samples were prepared by ion exchange. The exchange was performed by dropwise addition of a dilute solution containing M^{2+} ions to a slurry of NaY (Linde LZY-52) in doubly deionized water (DDW), 200 ml DDW per gram of NaY. The pH's for the Mg^{2+} and the Ca^{2+} exchanges were maintained at neutral for 24 h. The loadings of both Mg^{2+} and Ca^{2+} corresponded to approximately 16 ions per unit cell (equivalent to 32 Na^+ ions). After being washed with DDW, the samples were dried in air and then heated *in vacuo* up to 500°C at a heating rate of 10°C/h.

Subsequent Pd^{2+} ion exchange was carried out similarly with a $Pd(NH_3)_4^{2+}$ solution, leading to a Pd loading of the zeolite of approximately 9 Pd ions per unit cell (5 wt%). At the end of the preparation, only 5% of the original Na^+ ions are retained in the samples.

B. Temperature-Programmed Reduction (TPR)

Each sample (120 mg) was calcined to 500°C at 0.5°C/min under a flow of O_2 maintaining a high flow rate of 180 ml/min. Temperature-programmed reduction was performed at 8°C/min under a flow of 5% H_2 in Ar from −60 to 540°C. More details of the TPR experiments have been described previously (*28*).

C. FTIR

Each sample (20 mg) was pressed into 10-mm-diameter wafers for FTIR studies. Two transmission spectra were recorded for each sample: one after calcination at 200°C and another after calcination at 500°C. This procedure was chosen because our previous results had established that more than two ammine ligands per Pd are retained after calcination at 200°C, but oxidation of the

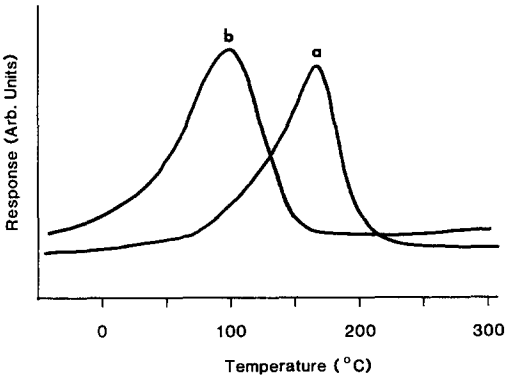

FIG. 1. Temperature-programmed reduction profiles of (a) PdNaY and (b) PdMgY.

ammine ligands was complete at T_c = 500°C (*29*). The two modes, (a) calcination up to T_c = 200°C and (b) calcination up to T_c = 500°C, thus represent the two extreme cases of complete proton neutralization by retained ammine ligands after reduction and complete Brønsted acidity of two H^+ per Pd^0 in the reduced zeolite, respectively. The calcinations were carried out at a heating rate of 0.5°C/min from 20°C to the specified temperature, T_c, and held at T_c for 2 h. This calcination was followed by (1) Ar purge at T_c for 20 min, (2) cooling in Ar to 20°C, (3) reduction at a rate of 8°C/min from 20 to 250°C and holding at 250°C for 20 min, (4) Ar purge at 250°C for 20 min, and (5) cooling in Ar to 20°C. Each sample will be denoted as Pd*M*–*T*; that is, PdCa-500 represents a Y zeolite supported palladium/calcium sample calcined at 500°C and subsequently reduced at 250°C for 20 min.

A Nicolet 60SX single-beam FTIR spectrometer with a spectral resolution of 1 cm^{-1} was used in the transmission mode. The samples were placed into a specially designed cell for *in situ* pretreatment. A background spectrum was collected for each sample before it was exposed to a flow of carbon monoxide (1 atm) for 10 min. After admission of CO, a flow of Ar was introduced to purge CO during data collection. Transmission FTIR spectra after CO adsorption were subtracted from the background spectrum. Further experimental details have been described in previous papers (*25*, *26*).

III. RESULTS

The most remarkable result of the sample characterization by temperature-programmed reduction was that the TPR profiles of PdM^{2+}Y (M^{2+} = Mg^{2+} and Ca^{2+}) after T_c = 500°C both peaked at temperatures about 70°C lower than the TPR profile of PdNaY. The profiles of PdMgY and PdCaY did not differ significantly, and therefore, only the TPR profiles of PdMgY and PdNaY are shown in Fig. 1.

Figure 2 shows the FTIR spectra of PdMg-500. For each spectrum the time in minutes of the Ar purge after CO adsorption is indicated in the figure legend. For comparison, the spectra of PdMg-200 are shown in

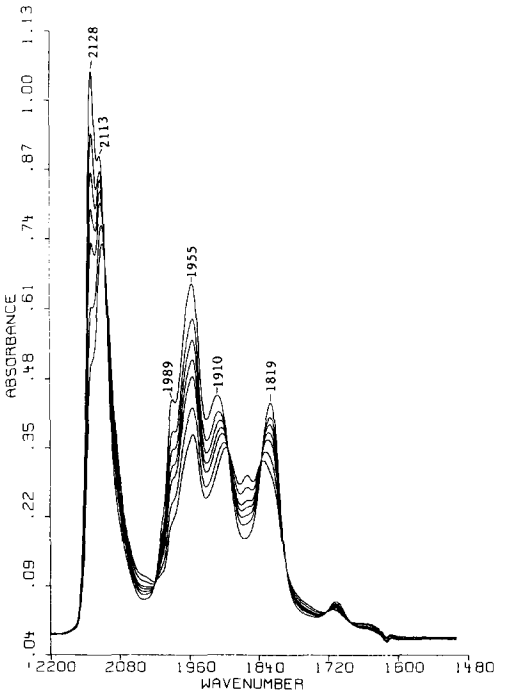

FIG. 2. FTIR spectra of CO adsorbed on PdMg-500 after different purging times with Ar at 25°C; purging time (min): 20, 30, 40, 50, 60, 80, 100 from top to bottom.

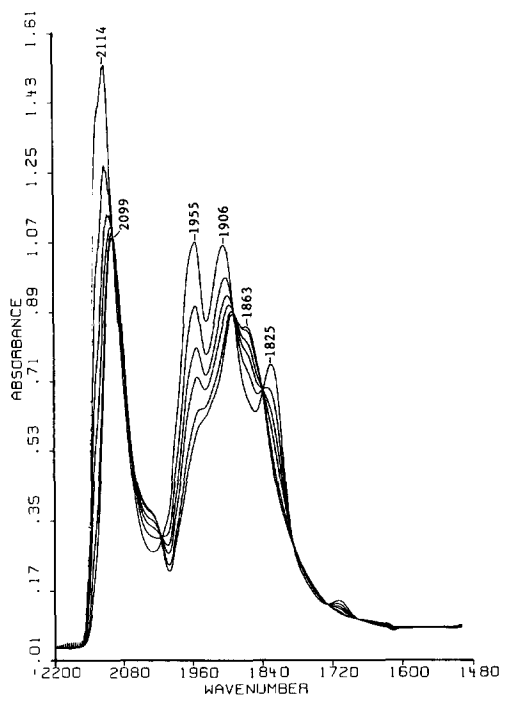

FIG. 3. FTIR spectra of CO adsorbed on PdMg-200 after different purging times with Ar at 25°C; purging time (min): 30, 40, 50, 60, 80, 100 from top to bottom.

Fig. 3. Whereas Fig. 2 shows two initial bands in the linear CO stretching region at 2128 and 2113 cm^{-1}, Fig. 3 shows only one band which appears at 2114 cm^{-1}. In addition, a band due to bridging CO appearing at 1989 cm^{-1} in Fig. 2 is absent in Fig. 3. Marked differences in other bridging CO bands between Figs. 2 and 3 are also obvious. Moreover, after purging for 100 min, the intensity of the linear CO band at 2128 cm^{-1} in Fig. 2 decreased significantly, whereas the other linear CO band at 2113 cm^{-1} decreased only slightly with no significant band shift. Conversely, the linear band in Fig. 3 shifted to 2099 cm^{-1} after purging for 100 min while its intensity decreased.

The spectra of PdCa-500 (Fig. 4) are similar to those of PdMg-500; they also show two initial absorption bands at 2132 and 2115 cm^{-1}, with the intensity of the 2132-cm^{-1} band decreasing rapidly during the Ar purge. After 100 min of purging, the linear band at 2107 cm^{-1} became the predominate band. In the bridging CO region, there are initially five bands at 1982, 1958, 1913, 1825, and 1717 cm^{-1}. During the Ar purge, the intensities of these five bands decreased and a new band at 1897 cm^{-1} became apparent. For comparison, the spectra of PdCa-200 are shown in Fig. 5. An apparent difference between both figures is that Fig. 5 shows only one linear band at 2115 cm^{-1}, whereas Fig. 4 shows two linear bands. After purging in Ar for 100 min the band intensity decreased and the band shifted to 2102 cm^{-1}.

The difference spectra of OH absorption in Fig. 6,I are obtained by subtracting the background spectrum of sample PdCa-500 after reduction from the spectra after introduction of CO and purging for 20 min [Fig. 6,I(a)] and 240 min [Fig. 6,I(b)]. Similarly, for sample PdCa-200 the spectra are shown

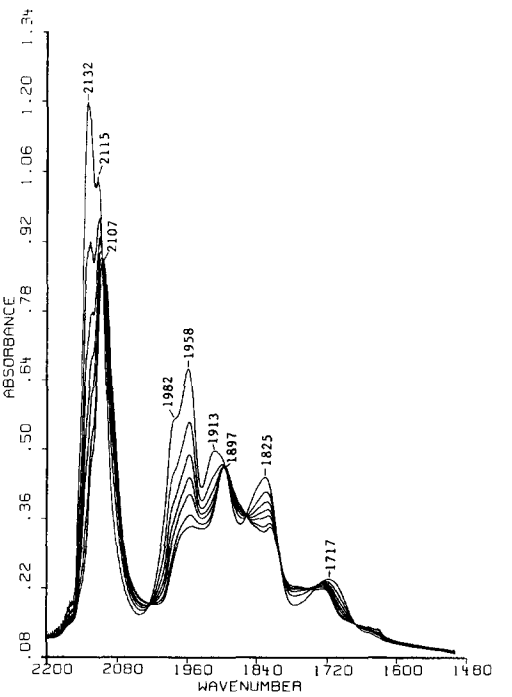

FIG. 4. FTIR spectra of CO adsorbed on PdCa-500 after different purging times with Ar at 25°C; purging time (min): 20, 30, 40, 50, 60, 80, 100 from top to bottom.

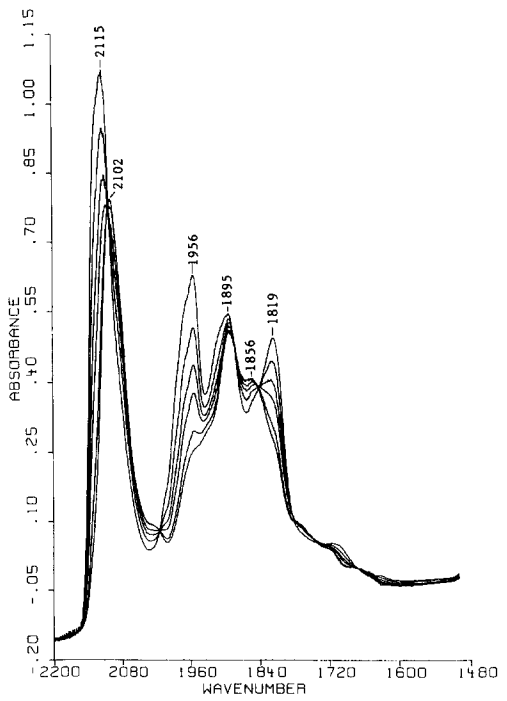

FIG. 5. FTIR spectra of CO adsorbed on PdCa-200 after different purging times with Ar at 25°C; purging time (min): 30, 40, 50, 60, 80, 100 from top to bottom.

in Fig. 6,II. The intensity of the bands in Fig. 6,I is much higher than that in Fig. 6,II.

IV. DISCUSSION

The distribution of Ca^{2+} and Mg^{2+} ions over different exchange sites in faujasite zeolites in hydrated and dehydrated samples has been the subject of much research (*30–32*). Recent X-ray diffraction work (*32*) has shown that Ca^{2+} and Mg^{2+} ions in hydrated samples occupy mainly $S_{I'}$, $S_{II'}$ and S_{II} sites, with Ca^{2+} having a higher distribution at $S_{I'}$ sites. In dehydrated samples, however, Mg^{2+} ions remain distributed among the above-mentioned sites, even though other spectroscopic techniques have detected that some Mg^{2+} ions occupy the S_I sites (*33*). These techniques have also shown that Ca^{2+} ions are preferentially located at S_I sites of faujasite zeolites in dehydrated samples (*30–32*).

The location of $Pd(NH_3)_x^{2+}$ ions in faujasite zeolites, particularly NaY, has been well characterized by X-ray diffraction (*34*), TPO, TPR (*35*), UV–VIS diffuse reflectance, and EXAFS (*29*). The conclusion is that the location of the Pd ions is determined strictly by the pretreatment conditions. For example, heating under inert gases or under vacuum induces autoreduction by the ammine ligands, leading to the formation of large particles (*36, 37*). Autoreduction can, however, be minimized by calcination under a high flow of oxygen (*35, 38*). The studies also showed that Pd ions retaining two or four ammine ligands are located in the zeolite supercages after calcination at 250°C. However, migration of Pd ions to $S_{I'}$ sites occurred above T_c = 300°C due to further oxidation of the am-

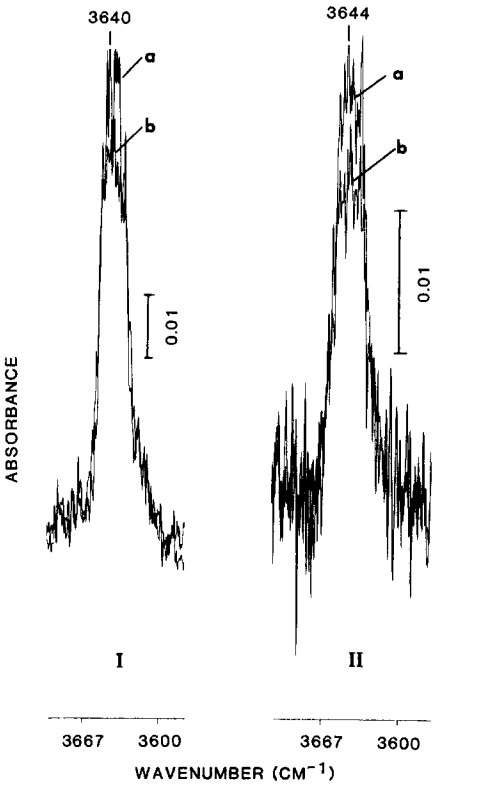

FIG. 6. Difference OH absorption spectra of (I) PdCa-500 after introducing CO and purging in Ar for 20 min (a) and 240 min (b) and (II) PdCa-200 after introducing CO and purging for 20 min (a) and 240 min (b).

mine ligands, with a minor fraction of the Pd ions migrating to the hexagonal prisms at even higher calcination temperatures (*29, 39, 40*).

The driving force for this migration is the higher density of negative charge in the smaller cages. When monovalent and multivalent ions coexist in the same faujasite zeolite, a state of lowest energy is characterized by a high concentration of multivalent cations in small cages. Once these cages have been filled with Mg^{2+} and Ca^{2+} ions, it is expected that the Pd^{2+} ions will remain at the $S_{II'}$ or the S_{II} sites. This is confirmed by the present TPR data: reduction of Pd in PdNa-500, in which Pd^{2+} ions occupy mainly the $S_{I'}$ sites, requires a temperature 70°C higher than that for the reduction of Pd in PdMg-500. We conclude from this remarkable result that Pd^{2+} ions in PdMg-500 are located in supercages. A site-blocking effect by divalent cations has been previously observed for the enhanced reduction of Ni^{2+} ions in zeolite Y, with Mn^{2+} ions as site blockers (*41*). Suzuki *et al.* reported that Mg^{2+} ions are less efficient than Ca^{2+} ions in blocking the hexagonal prisms for Ni^{2+} ions (*42*). For Pd^{2+} ions, however, blocking of sodalite cages with Mg^{2+} ions appears sufficient to retain Pd^{2+} ions in S_{II} and/or $S_{II'}$ sites. Pd^{2+} and Ni^{2+} differ in their site distributions upon dehydration. Ni^{2+} ions are known to be abundant in hexagonal prisms after high-temperature dehydration (*43*), but Pd^{2+} ions mainly occupy the sodalite cages (*29, 35, 44*). With Ca^{2+} ions blocking S_I and $S_{I'}$ sites, the Pd^{2+} ions are left to the remaining S_{II} and $S_{II'}$ sites. This explains why the TPR profiles for PdMg-500 and PdCa-500 are similar but they differ from that of PdNaY.

IR studies of CO on Pd single crystals show that "terminal" or "linear" CO absorption varies between 2090 and 2112 cm^{-1} depending on the type of crystal face (*45, 46*). Additionally, absorption bands of twofold bridging CO are at 1895 and 1878 cm^{-1} on Pd(100) and Pd(210), respectively (*45, 46*) and a band due to threefold bridging CO is at 1823 cm^{-1} (*47*). Furthermore, CO absorption bands between 2125 and 2130 cm^{-1} have been assigned to Pd^{+}–CO (*48*).

FTIR spectra of PdNa-500 were published previously and attributed to Pd carbonyl clusters (*22*). Their main features are: (1) a major band due to linearly adsorbed CO at 2120 cm^{-1}, (2) a pair of "butterfly" twofold adsorbed CO bands at 1969 and 1955 cm^{-1}, (3) a band corresponding to single CO bridging over two Pd atoms at 1898 cm^{-1}, and (4) a band corresponding to a single CO bridging over three Pd atoms at 1825 cm^{-1}. The FTIR spectra for PdNa-500 were reproduced for Pd loadings of 2 and 7 wt%.

As mentioned in the Introduction, attention is focused in the present work on indications for positively charged "electron-deficient" Pd_n particles. We assign the linear bands at 2128 cm^{-1} in Fig. 2 and at 2132 cm^{-1} in Fig. 4 to CO adsorbed on positively charged Pd. The adsorbent is assumed not to be a Pd^{+} ion since the wavenumbers of the doubly bonded CO band at 1982 cm^{-1} in PdCa-500 (Fig. 4) and 1989 cm^{-1} in PdMg-500 (Fig. 2) are significantly higher than those observed in PdNa-500 (*22*). Also, the band due to bridging, i.e., twofold adsorbed CO, is shifted from 1898 cm^{-1} for PdNaY to 1910 cm^{-1} for PdMg-500 and to 1913 cm^{-1} for PdCa-500. Both the terminal and the bridging CO are thus present on positively charged Pd in $Pd^{M^{2+}}Y$. Another observed difference between samples containing divalent charge-compensating ions, PdMg-500 and PdCa-500, and PdNa-500 (*22*) is that the geminal bands at 1969 and 1955 cm^{-1} for PdNa-500 are replaced by single bands at 1958 cm^{-1} for PdCa-500 and 1955 cm^{-1} for PdMg-500, respectively. All IR spectra thus consistently support our conclusion that the intense absorption bands of CO at high wavenumbers in PdMg-500 and PdCa-500 are due to a positive charge associated with Pd_n particles with $n > 1$.

Our results are in agreement with those of other recent spectroscopic studies of PdCaY and PdMgY which also detected a positively charged Pd species (*49–52*). The

possibility that the positive charge on Pd is due to incomplete reduction of Pd^{2+} ions in PdMg-500 and PdCa-500 can be ruled out on the basis of our TPR data; the integrated TPR profiles prove complete reduction of Pd^{2+} ions to Pd^0 in both samples. Since the reduction of a Pd^{2+} ion generates two protons, it appears reasonable to specify that some of these protons remain attached to the Pd_n particles. Our recent EXAFS results suggest that protons which are simultaneously interacting with Pd atoms and zeolite cage walls have an "anchoring" function which helps to stabilize them, preventing their migration and coalescence to large particles (*53*). These EXAFS data also showed that introduction of CO at room temperature resulted in an agglomeration of primary $Pd_n(CO)_x$ to form larger Pd particles with an average size of Pd_{13}. This observation is consistent with the model that the interaction between Pd_n and H^+ is weakened by CO adsorption.

The interaction of Pd clusters with CO ligands and protons is not only manifest from the FTIR spectra of CO, indicating Pd_{13} carbonyl clusters after migration and coalescence of the primary Pd carbonyl clusters at room temperature. Additional evidence is obtained from the OH band which illustrates the interaction of zeolite protons with either wall oxygen or Pd carbonyl. In particular the difference spectra shown in Fig. 6 reflect the changes in proton concentration and location. The absorption band at 3640 cm^{-1} has been assigned to the OH group inside supercages (*61*). The significant increase of this band when Pd carbonyls are formed after admission of CO can be attributed to the following processes:

$$(1)\ 13/n\ Pd_n\text{--}H^+\text{--}O_Z + x\ CO \rightarrow Pd_{13}(CO)_xH^+\text{--}O_Z + (13/n - 1)\ HO_Z$$

$$(2)\ Pd_{13}(CO)_xH^+\text{--}O_Z + CO \leftrightarrow Pd_{13}(CO)_{x+1} + HO_Z.$$

Process (1) involves an increase in nuclearity and has been found to be irreversible. The average nuclearity n of the primary particles varies with pretreatment conditions as determined by EXAFS spectroscopy (*62*). Therefore, the release of the protons from the primary proton adducts in the supercages is conceivably irreversible. Process (2) is an exchange of ligands of a Pd cluster and has been demonstrated to be reversible by monitoring the OH band (*26*). Protons and CO are thus ligands competing for the same cluster. The results of a comparison of PdCa-200 and PdCa-500 show that less protons are released for PdCa-200 because of their neutralization with ammonia retained in PdCa-200.

The main issue on which this discussion will further be focused is the problem: why is the interaction of zeolite protons with Pd clusters leading to electron-deficient particles so much more pronounced for PdMg-500 and PdCa-500 than for PdNa-500? We shall, therefore, consider the role of Mg^{2+} and Ca^{2+} during the reduction process. It should be pointed out that the presence of divalent cations such as Mg^{2+} and Ca^{2+} before reduction of Pd^{2+} ions has little effect on the proton concentration in the zeolite after reduction.

Basically, two possible models to describe the role of Mg^{2+} and Ca^{2+} can be discussed. The first model invokes a direct interaction of reduced metal clusters with Mg^{2+} and Ca^{2+} ions. Recent theoretical Hartree–Fock–Slater calculations show that the presence of Mg^{2+} in a zeolite pore causes an upward shift in the CO absorption band on Ir_4 clusters (*54*). This is attributed to a reduced repulsive interaction between the CO 5σ orbital and the Ir_4 clusters, and a decreased backdonation into the unoccupied CO $2\pi^*$ orbital as a result of the polarization of the Ir_4 clusters in the electrostatic field of Mg^{2+}. In general, electronegativity data of various cations including Ca^{2+}, Mg^{2+}, and Na^+ correlate with the acidity of corresponding zeolites (*55*).

A second model involves electron transfer from the metal clusters to acid sites (*56*). It has been speculated from infrared data that protons formed during hydrolysis of hy-

drated Ca^{2+} ions might act as electron acceptor sites (*9, 57, 58*); but those IR results did not conclusively differentiate between the two possible models.

A crucial factor for the solution of this problem is the novel finding that high *electron deficiency*, as evidenced by the CO FTIR data, and retention of Pd^{2+} in the supercages due to *site blocking* by M^{2+} ions, as evidenced by our TPR results, are related to each other. In the case of PdNa-500, Pd^{2+} ions are reduced in the sodalite cages; the neutral Pd atoms migrate into the supercages at high reduction temperature, leaving behind the protons which are the coproducts of Pd reduction.

Alternatively, for PdMg-500 and PdCa-500, the Pd^{2+} ions are located mainly in supercages even after high-temperature calcination because of site blocking by Mg^{2+} and Ca^{2+} ions. Consequently, the protons formed during reduction are located in the same supercages. Even though redistribution with Mg^{2+} or Ca^{2+} and H^+ may occur, there is no driving force to bring these protons to sodalite cages, where they would have to displace divalent cations. In the supercages, the stage is set for the formation of $[Pd_nH]^+$ adducts, via the following equilibrium:

$$Pd_n + HO_Z \rightleftharpoons Pd_n \rightarrow H\text{--}O_Z \rightleftharpoons [Pd_nH]^+ + O_Z.$$

Therefore, the conditions for the formation of the $[Pd_nH]^+$ adducts is much more favorable when Pd ions are retained in the supercages than when they can escape to the sodalite cages or hexagonal prisms. The high contribution of protons in supercages for PdMg-500 and PdCa-500 shifts the equilibrium to the right to form the metal–proton adducts. In view of the work by Védrine *et al.* (*12, 14, 21*), whereupon $Mg(OH)^+$ and $Ca(OH)^+$ were detected, protons generated by hydrolysis may further shift the equilibrium to the right.

Our proposed model, that site blocking leading to retention of Pd^{2+} ion in supercages is the crucial condition for the formation of the electron-deficient adducts, is in agreement with observations (*9, 20, 57–60*) that the effects of M^{2+} ions are limited by the high exchange level of Na^+ by M^{2+} ions. It is also easy to understand the effect of calcination temperature on the electron deficiency of reduced metal particles. CO IR spectra show only weakly polarized Pd clusters when T_c = 200°C. Protons formed during the reduction step are neutralized by NH_3 retained at a low calcination temperature of 200°C. Even if the bulky NH_4^+ ion does intereact with Pd_n clusters, it is expected to be considerably less polarizing than H^+.

We do not exclude possible interactions between Pd_n with Na^+ or NH_4^+. However, this type of interaction is expected to be much weaker than the interaction with the supercage protons. While NH_3 can be used to neutralize acidic HO_Z, it is of particular interest that recent efforts to convert the basic OH associated with $Mg(OH)^+$ and $Ca(OH)^+$ to acidic H+ have been successful when CO_2 was used (*12, 20*).

The shift of absorption bands with increasing Ar purging time as shown in Figs. 2–5 is similar to that observed previously for PdNaY (*22*), and this shift may be attributed to the relative stability of CO molecules adsorbed on different sites. Additionally, it is conceivable that the interaction between the Pd clusters with the protons is modified in the presence of CO. For example, as the CO molecules gradually release, the interaction with the protons responds accordingly. For small Pd particles (with an average of 13 atoms), a distortion or change of morphology may occur after a significant amount of CO is released. Summarizing, we conclude that $[Pd_nH]^+$ adducts or polarized, anchored Pd particles $Pd_n \rightarrow H\text{-}O_{ZS}$ (S standing for supercage) are the electron-deficient metal particles which were characterized in previous work by their enhanced catalytic activity. These particles coexist with protons of high Brønsted acidity in reduced Pd/zeolite catalysts. The role of the divalent ions, Ca^{2+} and Mg^{2+}, in favoring the forma-

tion of such "electron-deficient" particles is one cause of their catalyst promoter action in hydrocarbon conversion over such mono- and bifunctional catalysts.

ACKNOWLEDGMENTS

Financial support by the National Science Foundation (Contract CTS 8911184) and a grant-in-aid by the Mobil Foundation are gratefully acknowledged.

REFERENCES

1. Rabo, J. A., Pickert, P. E., Stamires, D. N., and Boyle, J. E., *in* "Proceedings, 2nd International Congress on Catalysis, Paris, 1960," p. 2055. Technic, Paris 1961.
2. Rabo, J. A., Pickert, P. E., and Mays, R. L., *Ind. Eng. Chem.* **53,** 733 (1961).
3. Topchieva, K. V., and Dorogochinskaya, V. A., *Dokl. Akad. Nauk SSSR* **208,** 1021 (1966).
4. Lanewala, M. A., Pickert, P. E., and Bolton, A. P., *J. Catal.* **9,** 2249 (1969).
5. Bolton, A. P., and Lanewana, M. A., *J. Catal.* **18,** 1 (1970).
6. Minachev, Kh. M., Garanin, V. I., Kharlamov, V. V., and Isakova, T. A., *Kinet. Catal.* **13,** 1104 (1972).
7. Kouwenhoven, H. W., *Adv. Chem. Ser.* **121,** 529 (1973).
8. Garanin, V. I., Kurkchi, U. M., and Minachev, Kh. M., *Kinet. Catal.* **9,** 1080 (1968).
9. Jacobs, P. A., and Uytterhoeven, J. B., *J. Chem. Soc. Faraday* **69,** 373 (1973).
10. Ben Taârit, Y., Bandiera, J., Mathieu, M. V., and Naccache, C., *J. Chim. Phys. Physicochim. Biol.* **67,** 37 (1970).
11. Moscou, L., and Moné, R., *J. Catal.* **30,** 417 (1973).
12. Mirodatos, C., Pichat, P., and Barthomeuf, D., *J. Phys. Chem.* **80,** 1335 (1976).
13. Plank, C. J., *in* "Proceedings, 3rd International Congress on Catalysis, Amsterdam, 1964," p. 727. Wiley, New York, 1965.
14. Ward, J. W., *Adv. Chem. Ser.* **101,** 380 (1971).
15. Uytterhoeven, J. B., Christner, L. G., and Hall, W. K., *J. Phys. Chem.* **69,** 2117 (1965).
16. Figueras, F., Gomez, R., and Primet, M., *Adv. Chem. Ser.* **121,** 480 (1973).
17. Mays, R. L., Pickert, P. E., Bolton, A. P., and Lanewala, M. A., *Oil Gas J.* **63,** 91 (1965).
18. Homeyer, S. T., Karpiński, Z., and Sachtler, W. M. H., *J. Catal.* **123,** 60 (1990).
19. Dalla Betta, R. A., and Boudart, M., *in* "Proceedings, 5th International Congress on Catalysis, Palm Beach, 1972" (H. Hightower, Ed.), p. 1329. North Holland, Amsterdam, 1973.
20. Jacobs, P. A., van Cauwelaert, F. H., Vansant, E. F., and Uytterhoeven, J. B., *J. Chem. Soc. Faraday Trans. 1,* 1056 (1973).
21. Abou-Kaïs, A., Mirodatos, C., Massardier, J., Barthomeuf, D., Vedrine, J. C., *J. Phys. Chem.* **81,** 397 (1977).
22. Sheu, L. L., Knözinger, H., and Sachtler, W. M. H., *J. Mol. Catal.* **57,** 61 (1989).
23. Ghosh, A., and Kevan, L., *J. Amer. Chem. Soc.* **110,** 8044 (1988).
24. Ghosh, A., and Kevan, L., *J. Phys. Chem.* **92,** 4439 (1988).
25. Sheu, L. L., Knözinger, H., and Sachtler, W. M. H., *Catal. Lett.* **2,** 129 (1989).
26. Sheu, L. L., Knözinger, H., and Sachtler, W. M. H., *J. Amer. Chem. Soc.* **111,** 8125 (1989).
27. Wong, T., Zhang, Z., and Sachtler, W. M. H., *Catal. Lett.* **4,** 365 (1990).
28. Zhang, Z., Sachtler, W. M. H., and Suib, S. L., *Catal. Lett.* **2,** 395 (1989).
29. Zhang, Z. Sachtler, W. M. H., and Chen, H., *Zeolites* **10,** 784 (1990).
30. Mortier, W. J., "Compilation of Extra-Framework Sites in Zeolites," Butterworths, Guildford, 1982.
31. Zverev, A. V., and Khvoshchev, S. S., *Izv. Acad. Nauk USSR Ser. Khim.* **10,** 2190 (1986).
32. Anderson, A. A., Shepelev, Y. F., and Smolin, Y. I., *Zeolites* **10,** 32 (1990).
33. Godber, J., Baker, M. D., and Ozin, G. A., *J. Phys. Chem.* **93,** 1409 (1989).
34. Bergeret, G., Gallezot, P., and Imelik, B., *J. Phys. Chem.* **85,** 411 (1981).
35. Homeyer, S. T., and Sachtler, W. M. H., *J. Catal.* **117,** 91 (1989).
36. Exner, D., Jaeger, N. I., Moller, K., and Schulz-Ekloff, G., *J. Chem. Soc. Faraday Trans. 1* **78,** 3537 (1978).
37. Moller, K., and Bein, T., *J. Phys. C* **8,** 231 (1986).
38. Homeyer, S. T., and Sachtler, W. M. H. *J. Catal.* **118,** 266 (1989).
39. Gallezot, P., and Imelik, B., *Mol. Sieves. Adv. Chem. Ser.* **121,** 66 (1973).
40. Michalik, J., Heming, M., and Kevan, L., *J. Phys. Chem.* **90,** 2136 (1986).
41. Jiang, H. J., Tzou, M. S., and Sachtler, W. M. H., *Catal. Lett.* **1,** 99 (1988).
42. Suzuki, M., Tsutsumi, K., Takahashi, H., and Yasukazu, *Zeolites* **9,** 98 (1989).
43. Gallezot, P., and Imelik, B., *J. Phys. Chem.* **77,** 652 (1973).
44. Bergeret, G., Gallezot, P., and Imelik, B., *J. Phys. Chem.* **85,** 411 (1981).
45. Bradshaw, A. M., and Hoffmann, F., *Surf. Sci.* **52,** 449 (1975).
46. Palazov, A., Chang, C. C., and Kokes, R. J., *J. Catal.* **36,** 338 (1975).
47. Bradshaw, A. M., and Hoffmann, F., *Surf. Sci.* **72,** 513 (1978).
48. Shubin, V. E., Shvets, A. A., Savel'eva, G. A., Popova, N. M., and Kazansky, V. B., *Kinet. Catal.* **27,** 1022 (1986).

49. Ashim, K. G., and Kevan, L., *J. Phys. Chem.* **92,** 4439 (1988).
50. Narayana, M., Michalik, J., Contarini, S., and Kevan, L., *J. Phys. Chem.* **89,** 3895 (1985).
51. Michalik, J., Narayana, M., and Kevan, L., *J. Phys. Chem.* **89,** 4553 (1985).
52. Baba, T., Nakano, K., Nishiyama, S., Tsuruya, S., and Masai, M., *Appl. Catal.* **52,** 81 (1989).
53. Zhang, Z., Chen, H., and Sachtler, W. M. H., *J. Catal.* (in press).
54. Jansen, A. P. J., and van Santen, R. A., *J. Phys. Chem.* **94,** 6764 (1990).
55. Mortier, W. J., *J. Catal.* **55,** 138 (1978).
56. de Mallmann, A., and Barthomeuf, D., *in* "Eleventh North American Meeting of the Catalysis Society, Dearborn, MI, 1989." [Abstract No. 11]
57. Uytterhoeven, J. B., Schoonheydt, R. A., Liengme, B. V., and Hall, W. K., *J. Catal.* **13,** 425 (1969).
58. Ward, J. W., *J. Phys. Chem.* **72,** 4211 (1968).
59. Pickert, P. E., Rabo, J. A., Dempsey, E., and Schomaker, V., *in* "Proceedings, 3rd International Congress on Catalysis, Amsterdam, 1964." Wiley, New York, 1965.
60. Isakov, Y. I., Klyachko-Gurvich, A. L., Khodiev, A. T., Minachev, Kh. M., and Rubinstein, A. M., *in* "Proceedings, 4th International Congress on *Catalysis*, Moscow, 1968" (B. A., Kazansky, Ed.), Paper 56. Adler, New York, 1968.
61. Breck, D. W., *in* "Zeolite Molecular Sieves," p. 475. Wiley, New York, 1984.
62. Zhang, Z., Chen, H., and Sachtler, W. M. H., submitted for publication.